Wing Rock Generated by Forebody Vortices

L. E. Ericsson*
Lockheed Missiles & Space Company, Inc., Sunnyvale, California

An analysis is performed of experimental results showing that at high angles of attack wing rock occurs for a tapered wing of aspect ratio 4, provided it is preceded by a slender ogive-cylinder body. In spite of the rather large wing span and associated roll damping, the wing rock is more violent than for a delta wing with highly swept leading edges. This surprising result is found to be caused by the critical flow conditions existing on the slender forebody, allowing the "moving-wall" effect on boundary-layer transition to generate the switching from symmetric to asymmetric separation and thus producing the vortex asymmetries needed to cause the observed wing rock.

Nomenclature

c = center chord of delta wing
d = diameter of cylindrical aft body
d^1 = sectional drag, coefficient $c_d = d^1/(\rho_\infty U_\infty^2/2)d$
l = sectional lift, coefficient $c_l = 1/(\rho_\infty U_\infty^2/2)d$
l_N = length of slender nose
p = body spin rate
Re = Reynolds number, $= U_\infty d/\nu_\infty$
t = time
U = velocity
x = axial distance from apex
Y = side force, coefficient $C_Y = Y/(\rho_\infty U_\infty^2/2)\pi d^2/4$
α = angle of attack
Δ = amplitude and increment
θ_A = apex half-angle
Λ = leading-edge sweep angle
ν = kinematic viscosity
ρ = air density
φ = meridional coordinate from stagnation point (Fig. 9)
ϕ = roll angle
ψ = coning rate (Fig. 19)

Subscripts

F = forebody
N = nose tip
W = wall
WR = wing rock
1,2,3 = numbering subscripts
∞ = freestream conditions

Introduction

RECENT experimental results[1] (Fig. 1) indicate that the wing rock induced by forebody vortices is more violent than that induced by the leading-edge vortices on a slender ($\Lambda = 80$ deg) delta wing[2] (Fig. 2), with the buildup to the 30–40 deg limit cycle amplitude occurring over less than 3 cycles rather than approximately 10. Flow visualization pictures taken during the wing rock (Fig. 3) show, according to the authors, the same type of asymmetry switching of the vortices as for the slender delta wing.[2] Based on the observed sensitivity to forebody geometry of the asymmetric vortex phenomenon,[3,4] a number of forebody geometries were tested[1] (Fig. 4). The results were rather surprising[1] (Fig. 5). Only the chine configuration showed a substantial change of the wing rock amplitude, especially for the "cleaner" wing-body configuration (Fig. 5b). The other geometric shapes had surprisingly similar wing rock characteristics. The fluid mechanical reason for this will be discussed.

Figure 3 shows clearly that the wing rock is not caused by some interaction between the wing and the vortex generation on the nose. The wing simply provides the downstream surfaces needed for generation of the rolling moment driving the wing rock. That is, the situation is similar to the one leading to body rock[5] (Fig. 6). There is, however, one big difference. In the present case, there is no forebody asymmetry, such as the cockpit in Fig. 6, to cause the asymmetry switching. Thus, a more general flow mechanism for asymmetry switching than the one discussed in Ref. 5 must exist. What this flow mechanism is will be discussed in the next section.

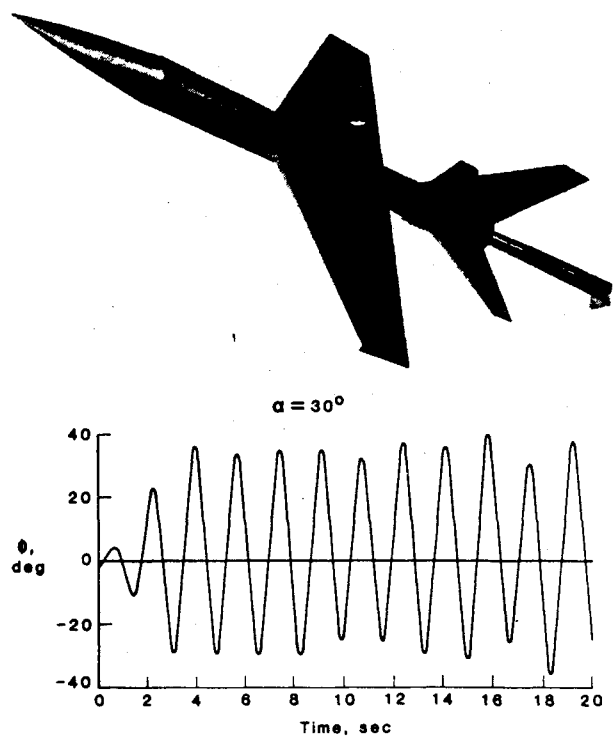

Fig. 1 Wing rock buildup at $\alpha = 30$ deg for horizontally elliptic forebody.[1]

Received Dec. 11, 1986; presented as Paper 87-0268 at the AIAA 25th Aerospace Sciences Meeting, Reno, NV, Jan. 12–15, 1987; revision received Sept. 6, 1988.

*Senior Consulting Engineer. Fellow AIAA.

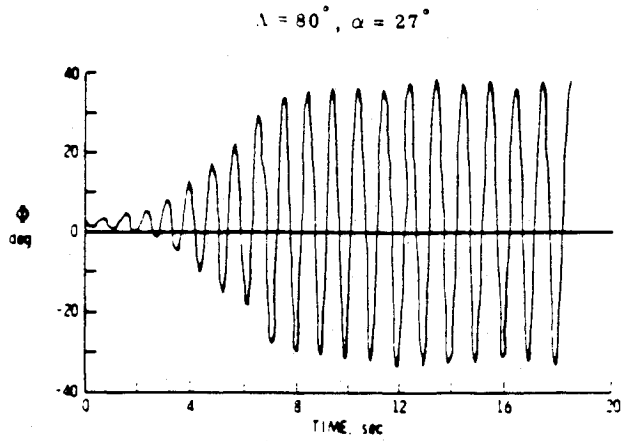

Fig. 2 Wing rock buildup at $\alpha = 27$ deg for an 80 deg delta wing.[2]

Motion-Induced Asymmetry Switching

A flow mechanism able to cause a switching of the cross-flow separation geometry has been described before.[6] Figure 7 shows experimental Magnus lift results for initially laminar flow conditions[7] (at $U_W = 0$). Below $U_W/U_\infty = 0.3$, the Magnus lift is generated mainly by the downstream moving-wall effect on the top side, moving the separation from the subcritical toward the supercritical position. On the bottom side, the separation is already of the subcritical type at $U_W = 0$ and the upstream moving-wall effect does not have much leverage for its separation-promoting action. When the rotation rate is increased beyond a critical value, a so-called Magnus lift reversal occurs. The critical value of U_W/U_∞ depends on the Reynolds number, being U_W/U_∞ 0.3 for $Re = 0.128 \times 10^6$. This lift reversal is caused by the moving-wall effect on boundary-layer transition. When $p > p_{crit}$, the upstream moving-wall effect on the bottom side causes boundary-layer transition to occur before separation, changing it from the subcritical toward the supercritical type. This effect completely overpowers the regular moving-wall effects on separation and causes a more or less discontinuous loss of lift (Fig. 7). When the Reynolds number is increased to $0.26 \times 10^6 \leq Re \leq 0.325 \times 10^6$, the critical U_W/U_∞ value approaches zero,[6,7] explaining the very large effect of infinitesimal spin rates for a spinning nose tip[8,9] (Fig. 8).

In the critical Reynolds number region, the moving-wall effects on flow separation and associated forebody vortices are complicated by the presence of a laminar separation bubble[10,11] (Fig. 9). The laminar flow separation develops near the lateral meridian ($\varphi = 90$ deg) and is followed by a transition in the lifted shear layer that causes flow reattachment. The reattaching turbulent boundary layer is able to withstand the adverse pressure gradient until $\varphi = 140$ deg before the final flow separation occurs. This is far aft of the separation location for a fully turbulent boundary layer, $\varphi \approx 100$ deg, resulting in a "drag bucket" for the critical Reynolds number region.[10,11] (See Fig. 9.)

When the Reynolds number is increased, transition moves forward in the bubble shear layer, resulting in a delay of the final turbulent flow separation. This beneficial effect of the increasing Reynolds number continues until transition reaches the top of the bubble, where it will remain until the Reynolds number has been increased enough to overcome the transition delay caused by local accelerated flow effects. The minimum drag plateau in Fig. 9 would result from such momentary arrest of the forward transition movement with increasing Reynolds number. When the Reynolds number is increased further, the transition jumps forward of the bubble, wiping it out. The resulting supercritical type separation increases with increasing Reynolds number, resulting in increased drag (Fig. 9).

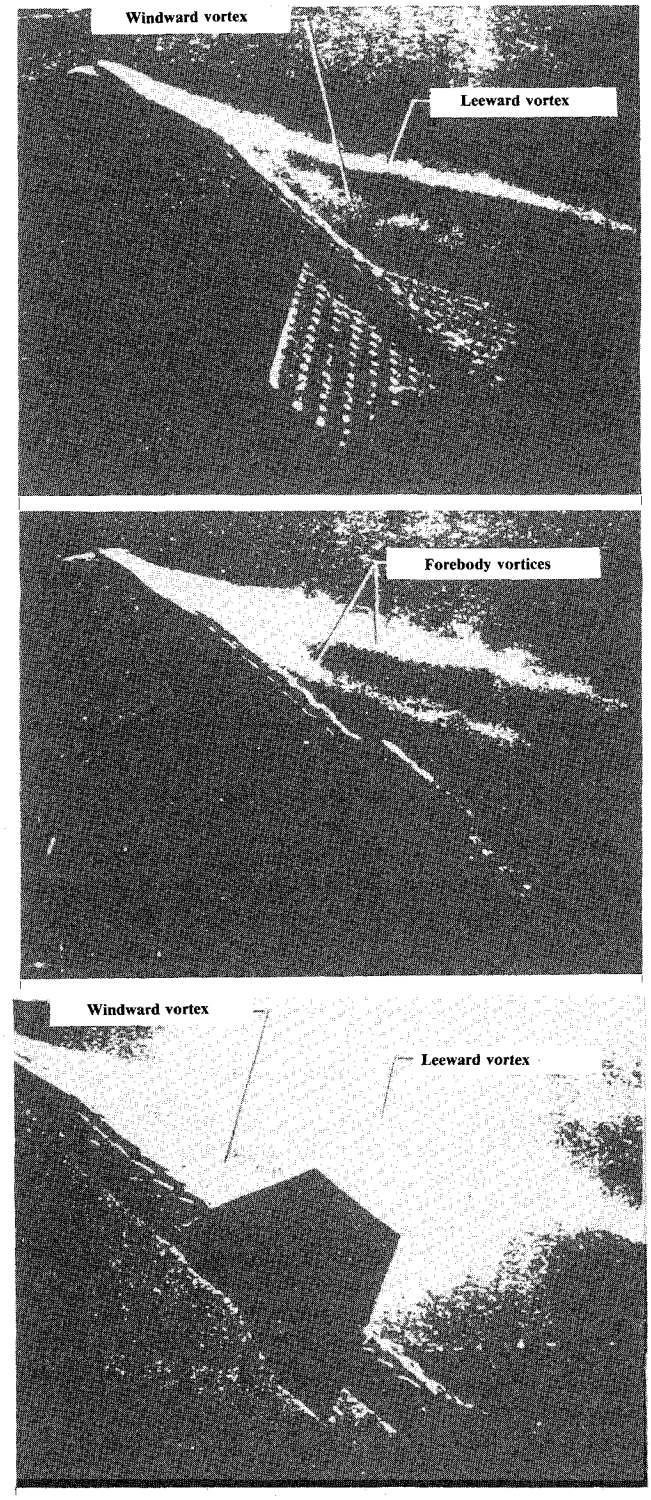

Fig. 3 Smoke flow patterns during wing rock at $\alpha = 35$ deg for horizontally elliptic forebody.[1]

The first part of the critical flow region in Fig. 9, with its sharp drop of the drag with increasing Reynolds number until the minimum drag plateau is reached, corresponds to the Reynolds number region in Fig. 10, producing the experimentally observed negative Magnus lift slope.[7]

In the case of the rotating circular cylinder (Fig. 11b), the upstream moving-wall effect is equivalent to the effect of increasing the Reynolds number and causes a forward movement of transition in the lifted shear layer forming the laminar separation bubble. As is sketched in Fig. 11b, the resulting delay of the final turbulent flow separation produces increased

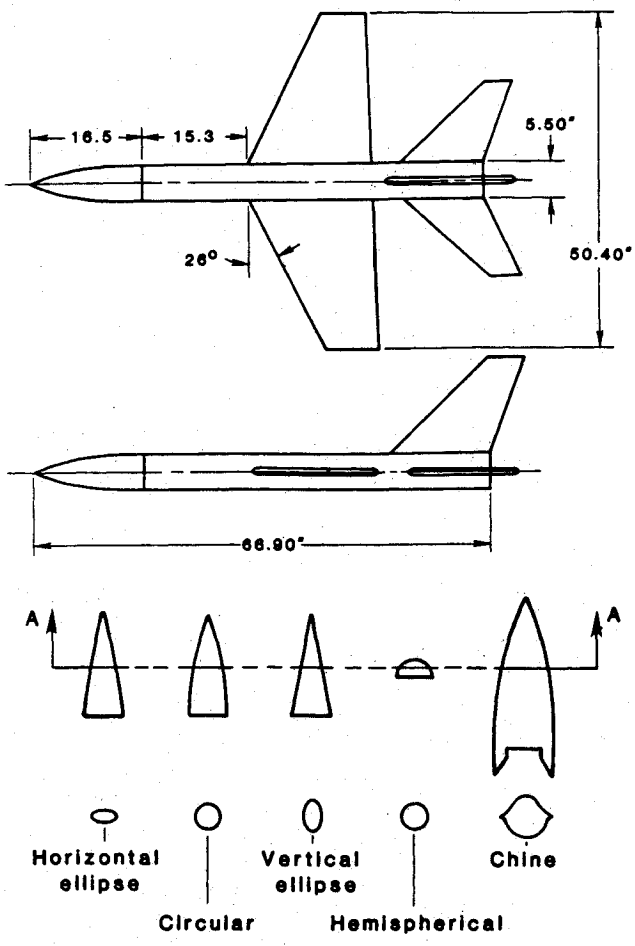

Fig. 4 Tested model geometries.[1]

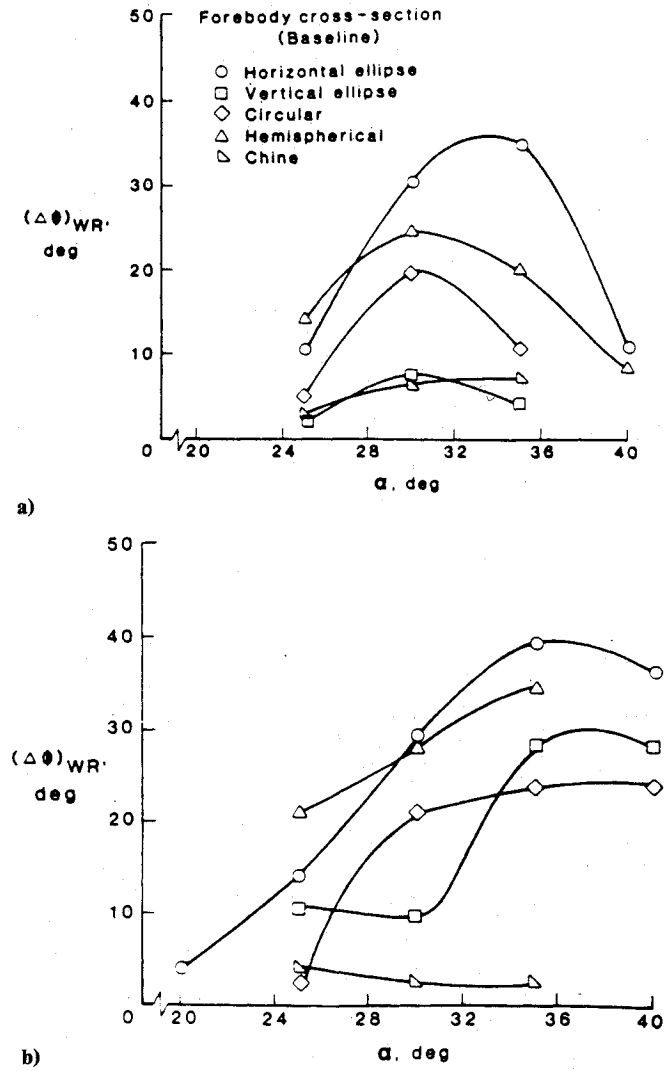

Fig. 5 Effect of forebody shape on wing rock amplitude[1]: a) complete configuration, b) tail surfaces removed.

suction, generating most of the measured negative Magnus lift shown in Fig. 10. A comparatively smaller contribution to the negative Magnus lift is generated by the transition delay, caused by the downstream moving-wall effect on the opposite side, which promotes (the final turbulent) flow separation and causes a loss of suction.

That is, the influence of the upstream and downstream moving-wall effects on the two sides of the rotating cylinder is similar to that of increasing and decreasing, respectively, the Reynolds number on the two separate sides. At critical flow conditions, this effective change of the Reynolds number means sliding down and up, respectively, on the steep drag slope in Fig. 9, producing a corresponding large change of the Magnus lift, illustrated by the results[7] in Fig. 10.

Nose-Induced Wing Rock

The Reynolds number based the body diameter in the test performed by Brandon and Nguyen[1] was $Re = 0.26 \times 10^6$. The crossflow over the nose and nose shoulder will, therefore, be in the critical Reynolds number region just discussed, providing the following scenario. (See Fig. 12.) At $t = t_1$, the adverse upstream moving-wall effect on the forebody crossflow causes boundary-layer transition to occur earlier in the shear layer of the laminar separation bubble, in the manner just discussed in the case of the generation of negative Magnus lift (Fig. 10). This effect is similar to that of changing the flow separation from the subcritical toward the supercritical type. In the absence of time lag effects, the vortex geometry sketched at $t = t_1$ will result. Due to time lag effects similar to those discussed in Ref. 12, this vortex geometry is not realized until $t = t_1 + \Delta t$. (Only the lower vortex is shown as only it will induce significant loads on the wing-body configuration.) At $t = t_3$, when the roll rate reaches its maximum in the opposite direction, another forebody switch in separation asymmetry occurs. Because of the time lag effect,[12] the vortex geometry at the (now horizontal) wing has not changed, but is the same as at $t = t_1 + \Delta t$, in agreement with the flow pictures in Fig. 3. During the time lag Δt, the vortex induced rolling moment drives the rolling motion, generating the observed wing rock.

Amplitude Buildup

The excellent flow visualization results obtained by Keener[13] (Fig. 13) show the finite extent on an ogival nose of the transitional separation region with its laminar separation bubble. This finite extent is in agreement with the finite Reynolds number range for which the critical flow region with its negative Magnus lift exists for a rotating circular cylinder[7] (Fig. 10). This provides the following explanation for the much faster amplitude buildup in the present case of asymmetric forebody vortices (Fig. 1) than in the case of asymmetric delta wing leading-edge vortices (Fig. 2).

When the free-to-roll model in Fig. 1 responds to some disturbance, a flow asymmetry with associated asymmetric vortex pair is generated. The wing rock, resulting from the vortex-induced loads on the wing-body, will grow very fast in amplitude from half-cycle to half-cycle. The peak moving wall

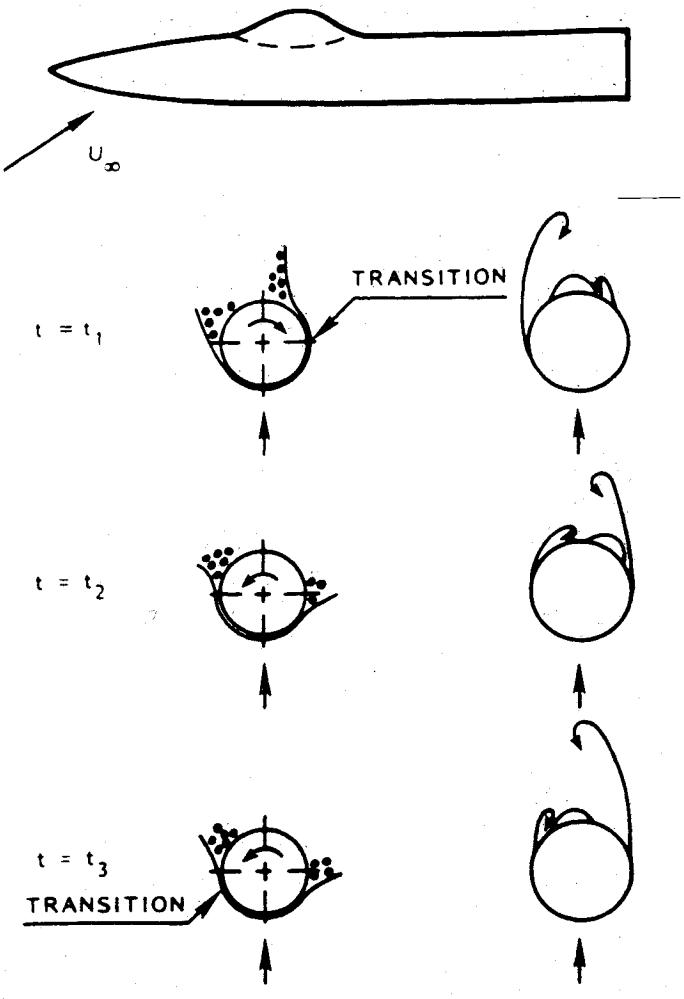

Fig. 6 Conceptual flow mechanism for body rock.[5]

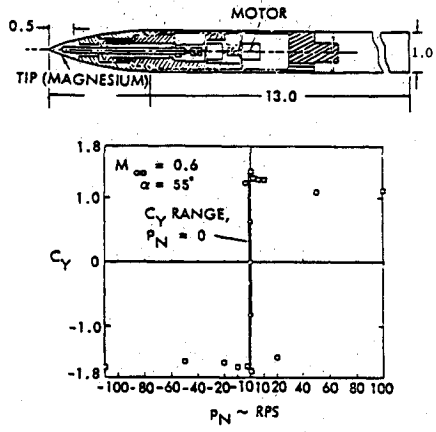

Fig. 8 Effect of spinning nose tip on separation-induced side force.[9]

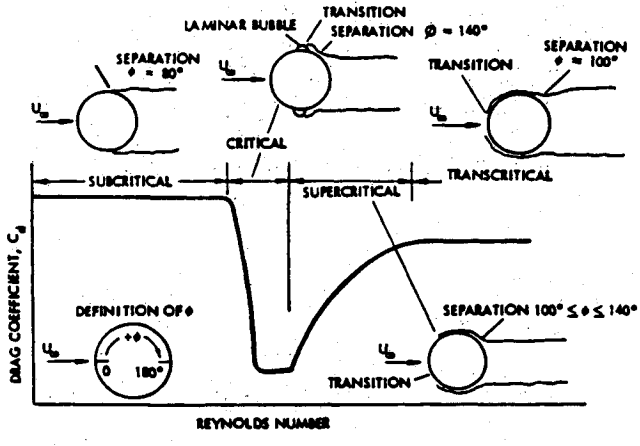

Fig. 9 Flow regions for a circular cylinder.[10]

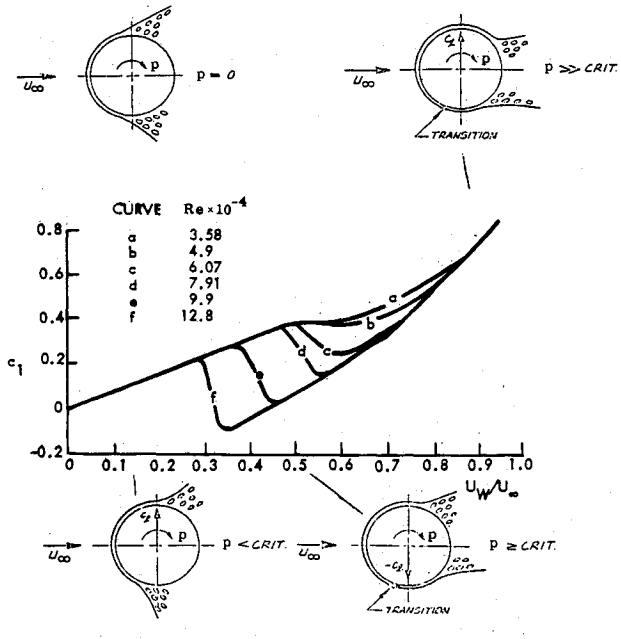

Fig. 7 Moving-wall effects on transition and separation.[6]

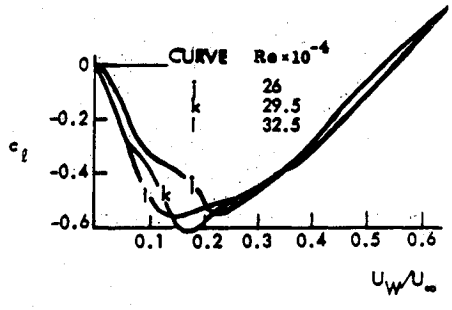

Fig. 10 Measured Magnus lift on a rotating cylinder at critical flow conditions.[7]

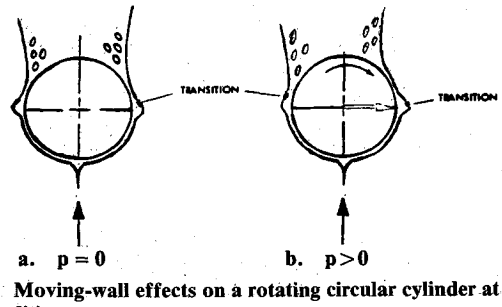

Fig. 11 Moving-wall effects on a rotating circular cylinder at critical flow conditions.

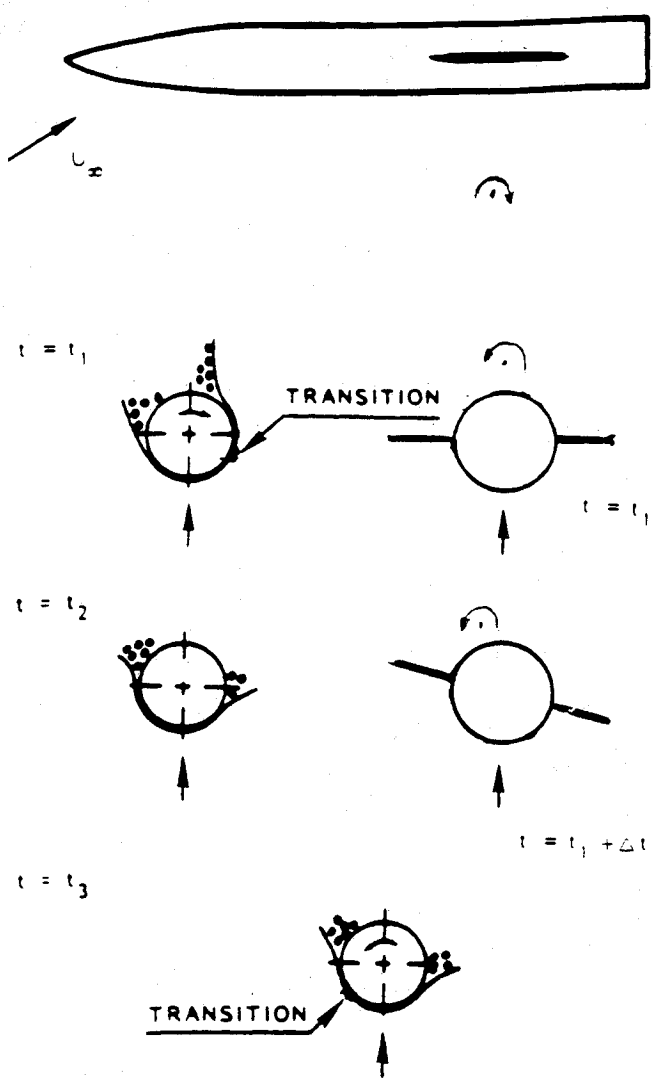

Fig. 12 Conceptual flow mechanism for wing-body work.

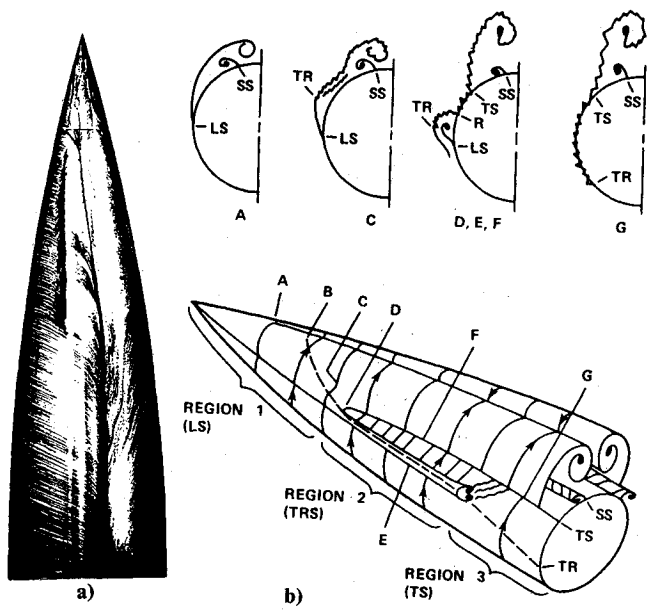

Fig. 13 Flow visualization results for a pointed 3.5 ogive at $M = 0.25$ and $\alpha = 55$ deg[13]: a) oil flow visualization, camera at $\varphi = 135$ deg; b) flow model.

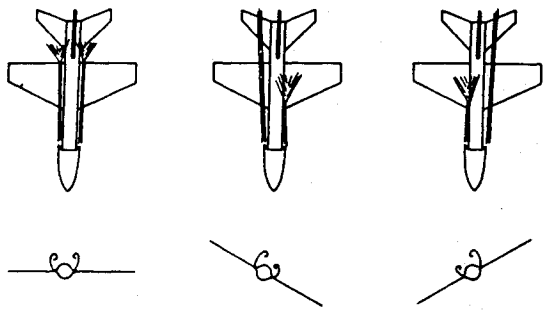

Fig. 14 Observed vortex characteristics for chined forebody at $\alpha = 35$ deg.[1]

velocity is proportional to the amplitude $\Delta\phi$. Thus, the flow separation asymmetry, and with it the strength of the asymmetric vortex inducing the wing loads, will grow with increasing amplitude due to the increase of the moving-wall effect described in connection with Figs. 9–11.

Something needs probably to be said in regard to the unusual power of the moving-wall effects in the present case, where the moving-wall velocity is only a few percent of the freestream velocity. For the wing rock in Fig. 1, with a frequency of approximately 0.6 Hz and an amplitude $\Delta\phi \approx 35$ deg, one obtains $|U_W/U_\infty| \leq 0.014$. In regard to the spinning nose tip in Fig. 8, there was some question in regard to the validity of data obtained for $p_N < 5$ Hz, because of the 5 Hz filter used.[9] Even for $p_N = 5$ Hz, however, the moving-wall velocity on the spinning nose tip did not exceed $|U_W/U_\infty| = 0.0125$. Thus, when considering the fact that the moving-wall effect acts over a much larger axial extent of the body in the case of the wing rock (Fig. 1) than in the case of the spinning nose tip (Fig. 8), the postulated moving-wall effects for the wing rock appear reasonable.

One important observation to be made is that, when the Reynolds number is increased, the axial extent of the critical flow region decreases. Thus, one would expect the wing rock generated by forebody vortices in full-scale flight to be milder than the one experienced in subscale tests, where the axial extent of the critical flow region is larger. Of course, if the test Reynolds number is low enough to cause laminar flow conditions over the complete ogive-cylinder body, the subscale test would not give any hint of the wing rock to be expected in full-scale flight, based on the wing-rock-generating flow mechanism presented here. Obviously, further systematic tests of the type described in Ref. 1 are needed.

Effect of Forebody Geometry

Changing the forebody cross section from circular to horizontally elliptic (Fig. 4) increased the wing rock amplitude (Fig. 5b). This can be expected, as the apex half-angle in the α plane decreases from

$$\theta_A = \tan^{-1} \frac{l_N/d}{(l_N/d)^2 - 0.25} = 19 \text{ deg}$$

for the $l_N/d = 3$ circular tangent-ogive[14] to $\theta_A = 15$ deg for the horizontally elliptic nose tip.[1] That causes vortex shedding to start earlier on the elliptic nose. Figure 5b shows clearly the effect of this earlier start.

Applying the same reasoning to the vertically elliptic cross section, one would expect a decrease of the wing rock amplitude. The experimental results show this decrease relative to the horizontally elliptic cross section. However, no such consistent trend exists relative to the circular cross section. It appears that two different vortex-induced lift-generating mechanisms may have been present. Further analysis has indeed shown this to be the case.[15]

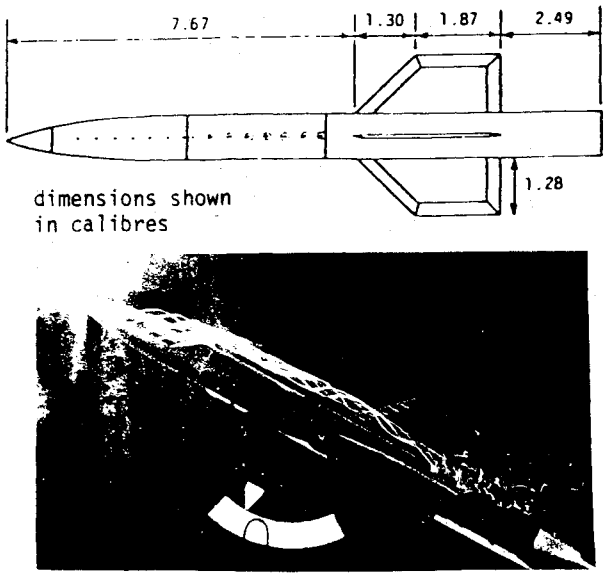

Fig. 15 Wing-induced burst of forebody vortices.[17]

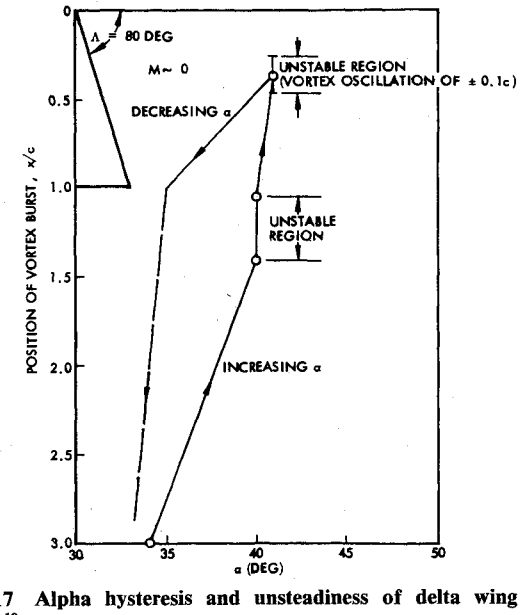

Fig. 17 Alpha hysteresis and unsteadiness of delta wing vortex burst.[19]

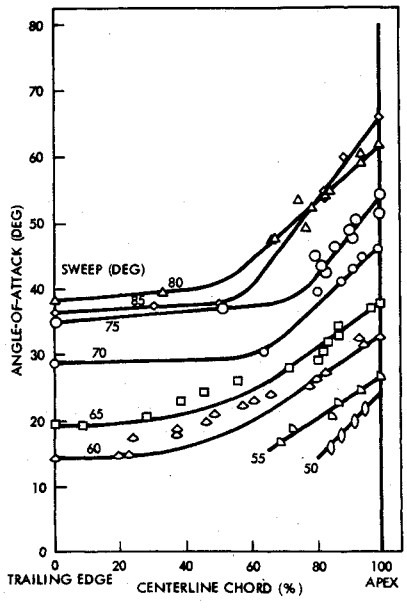

Fig. 16 Delta wing vortex burst characteristics.[18]

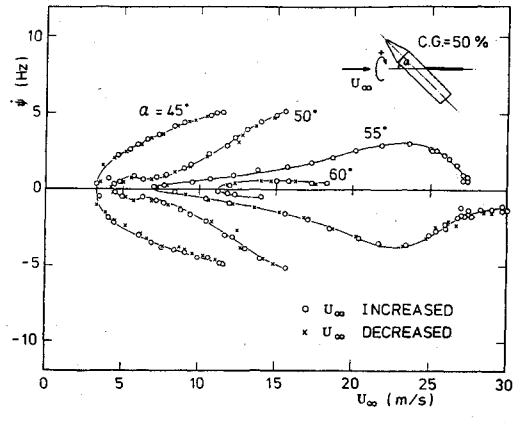

Fig. 18 Equilibrium coning rates of a cone-cylinder body.[21]

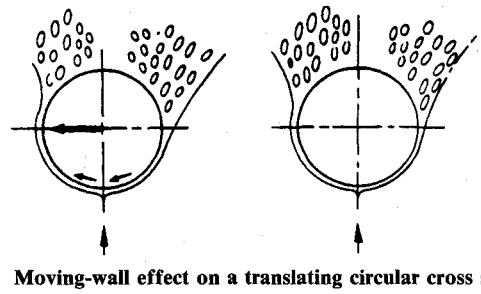

Fig. 19 Moving-wall effect on a translating circular cross section.[8]

For the hemispherical nose, the body vortices will be generated on the cylindrical forebody, following the established blunt-body behavior.[14] Without accounting for wing-induced upwash, the body vortices will start at the position of the wing leading edge at $\alpha \approx 22$ deg according to Fiechter's experimental results.[16] Because of the effect of the upwash, the vortices will start well ahead of the wing leading edge at $\alpha = 22$ deg and the starting point will move forward further with increasing angle of attack. Even so, the vortices will be closer to the wing than those generated by the pointed ogival nose, which explains the experimentally observed large wing rock amplitude for the hemispherical nose (Fig. 5). It should be noted that, for the test Reynolds number $Re = 0.26 \times 10^6$, critical flow conditions are established on the circular cylinder (see Fig. 10).

The only forebody change that had a substantial impact on the wing rock was the one made to a chined body cross section (Fig. 5). The chine should act as a forebody strake, fixing flow separation and the associated vortex shedding. The causative mechanism is, therefore, probably associated with the vortex burst observed in the test[1] (Fig. 14). However, it cannot be the burst interaction with the wing-body juncture that causes wing rock. It has the wrong aerodynamic characteristics, as has been discussed at length for a slender delta wing.[12]

Whereas the sketch at $\alpha = 0$ in Fig. 14 is in agreement with other experiments[17] (Fig. 15), the sketches for $\alpha > 0$ are probably not realistic. Figure 5 shows that the roll amplitude never exceeded 5 deg. Another characteristic for the chine configuration in Fig. 5b, which distinguishes it from the others, is the insensitivity to angle of attack of the wing rock amplitude. This is in agreement with the observed "hang-up" of vortex

burst at the trailing edge, causing a jump forward to the midwing position when the burst finally occurs on the wing[18] (Fig. 16). Considering further the associated burst unsteadiness[19] (Fig. 17), one feels inclined to believe that the low-amplitude wing rock experienced by the chine configuration[1] is simply the wing-body response to this unsteady vortex burst. That is, it is not of the self-excited type experienced by the other configurations. This would explain both the small wing rock amplitude and its α-insensitivity. Any coupling with the body motion of the vortex burst would be damping[12] and may, in fact, have been a factor in limiting the wing rock amplitude, as in the case of slender wing rock.[20]

Free Flight

The experimentally observed wing rock[1] was obtained on a model that had only the roll degree of freedom. For an aircraft or missile in free flight, the asymmetric flow separation with associated vortices is likely to generate a large yawing moment and also to affect the pitching moment. That is, one can expect a strong coupling between the three angular degrees of freedom. Some appreciation for this can be obtained by studying test results for a cone-cylinder model[21] describing a coning motion at high angles of attack (Fig. 18). The authors describe how only a slight initial push was needed to establish the coning motion in one direction or the other, regardless of the fact that the measured static yawing moment at zero side slip was biased in one direction due to nose microasymmetries.[3,4,14] The body reached nearly equal steady-state coning rates in both directions (Fig. 18). That is, the motion dominated over the static asymmetry, locking in the asymmetry in the direction of the body motion; thus driving the motion. This is a result of the moving-wall effects on flow separation,[8] as is illustrated in Fig. 19. The translatory motion of the circular cross section causes flow separation to be delayed on the advancing side and promoted on the retreating side. Thus, the motion generates a separation-induced force that drives it until the equilibrium coning rate is reached, at which point the driving moment is balanced by the damping due to the drag moment, similar to the case of flat spin.[11]

Two things are worth emphasizing when trying to apply these results to full-scale vehicle design. One is that, for vehicles with long slender noses, the critical flow conditions will occur within a large Reynolds number region above Re_{crit}. The other observation is that fixes like a flattening of the slender nose, which greatly diminish the asymmetry-induced side force and associated yawing moment,[22] could increase the roll response due to vortex interaction with downstream lifting surfaces (as is shown in Fig. 5).

Conclusions

An analysis of the experimentally observed wing rock on a wing-body configuration shows the following:

1) The rocking motion is caused by the wing-body response to asymmetric vortices generated on the slender nose cylinder body forward of the wing.

2) The main flow mechanism responsible for the switching of vortex asymmetry needed to drive the rocking motion is the moving-wall effect on forebody transition and associated asymmetric flow separation.

Acknowledgments

The results presented in this paper were in part developed under contract to the Air Force Flight Dynamics Laboratory/FIGC, Wright-Patterson AFB, Contract F33615-87-C-3607, monitored by W. B. Blake.

References

[1]Brandon, J. M. and Nguyen, L. T., "Experimental Study of Effects of Forebody Geometry on High Angle of Attack Stability," *Journal of Aircraft,* Vol. 25, July 1988, pp. 591–597.

[2]Nguyen, L., Yip, L., and Chambers, J., "Self-Induced Wing Rock of Slender Delta Wings," AIAA Paper 81-1883, Aug. 1981.

[3]Ericsson, L. E. and Reding, J. P., "Review of Vortex-Induced Asymmetric Loads—Part I," *Zeitschrift für Flugwissenschaten Weltraumforsch,* Vol. 5, No. 3, 1981, pp. 162–174.

[4]Ericsson, L. E. and Reding, J. P., "Review of Vortex-Induced Asymmetric Loads—Part II," *Zeitschrift für Flugwissenschatten Weltraumforsch,* Vol. 5, No. 6, 1981, pp. 349–366.

[5]Ericsson, L. E., "A Possible Causative Flow Mechanism for Body Rock," *Journal of Aircraft,* Vol. 22, May 1985, pp. 441–443.

[6]Ericsson, L. E., "Kármán Vortex Shedding and the Effect of Body Motion," *AIAA Journal,* Vol. 18, Aug. 1980, pp. 935–944.

[7]Swanson, W. M., "The Magnus Effect: A Summary of Investigations to Date," *Journal of Basic Engineering,* Vol. 83, Sept. 1961, pp. 461–470.

[8]Ericsson, L. E. and Reding, J. P., "Dynamics of Forebody Flow Separation and Associated Vortices," *Journal of Aircraft,* Vol. 22, April 1985, pp. 329–335.

[9]Fidler, J. E., "Active Control of Asymmetric Vortex Effects," *Journal of Aircraft,* Vol. 18, April 1981, pp. 267–272.

[10]Achenbach, E., "Influence of Surface Roughness on the Cross-Flow Around a Circular Cylinder," *Journal of Fluid Mechanics,* Vol. 46, Pt. 2, 1971, pp. 321–335.

[11]Ericsson, L. E., "Flat Spin of Axisymmetric Bodies in the Critical *Re*-Region," *Journal of Spacecraft and Rockets,* Vol. 24, Nov.–Dec. 1987, pp. 532–538.

[12]Ericsson, L. E., "The Fluid Mechanics of Slender Wing Rock," *Journal of Aircraft,* Vol. 21, May 1984, pp. 322–328.

[13]Keener, E. R., "Flow-Separation Patterns on Symmetric Forebodies," NASA TM 86016, Jan. 1986.

[14]Ericsson, L. E. and Reding, J. P., "Asymmetric Vortex Shedding from Bodies of Revolution," *AIAA Progress in Astronautics and Aeronautics: Tactical Missile Aerodynamics,* Vol. 104, edited by M. J. Hemsch and J. N. Nielsen, AIAA, New York, 1986, pp. 343–296.

[15]Ericsson, L. E., "Further Analysis of Wing Rock Generated by Forebody Vortices," AIAA Paper 88-2597, June 1988.

[16]Fiechter, M., "Über Wirbelsysteme an Schlanken Rotationskörpern und ihren Einfluss auf die aerodynamische Beiwerte," Deutsch-Französisches Forchungs-Institut, Saint Louis, France, Rept. 10/66, Dec. 1966.

[17]Deane, J. R., "Experimental Investigation into the Interaction Between Body Vortices and Wing Panels on a Missile Configuration at Low Speed," AIAA Paper 80-0032, Jan. 1980.

[18]Wendtz, W. H. and Kohlman, D. L., "Vortex Breakdown on Slender Sharp-Edged Wings," AIAA Paper 69-778, July 1969.

[19]Lowson, M. V., "Some Experiments with Vortex Breakdown," *Journal of the Royal Aeronautical Society,* Vol. 68, May 1964, pp. 343–346.

[20]Ericsson, L. E., "Analytic Prediction of the Maximum Amplitude of Slender Wing Rock," *Journal of Aircraft,* Vol. 26, Jan. 1989, pp. 35–39.

[21]Yoshinaga, T., Tate, A., and Inoue, K., "Coning Motion of Slender Bodies at High Angles of Attack in Low Speed Flow," AIAA Paper 81-2485, Aug. 1981.

[22]Skow, A. M., Titiriga, A., and Moore, W. A., "Forebody-Wing Vortex Interactions and Their Influence on Departure and Spin Resistance," AGARD CP-247, Jan. 1979, Paper 6.